



# Carbon Material With Ordered Sub-Nanometer Hole Defects

Nianjie Liang<sup>1†</sup>, Qiaosheng Li<sup>1†</sup>, Ganghuo Pan<sup>1</sup>, Chunxiang Liu<sup>1</sup> and Yuzhou Liu<sup>1,2,3\*</sup>

<sup>1</sup>School of Chemistry, Beihang University, Beijing, China, <sup>2</sup>Beijing Advanced Innovation Center for Biomedical Engineering, Beihang University, Beijing, China, <sup>3</sup>Beijing Shenyun Zhihe Technology Co., Ltd., Beijing, China

A holey carbon material with ordered sub-nanometer hole defects was synthesized from oxidative cyclodehydrogenation of a polyhexaphenylbenzene precursor. Band gap of around 2.2 eV is formed due to the narrow connection between the hexabenzocoronene subunits. It has weak interlayer interaction energy compared with graphene and shows easy dispersion in a wide range of solvents, surprisingly including water. Density functional theory calculations confirmed the excellent dispersion of this material in water. This new carbon material was then proved as effective support for various inorganic nanoparticles of small sizes. The supported iron nanoparticles showed enzyme-like catalysis behavior in nitrophenyl reduction reaction by NaBH<sub>4</sub>, exemplifying the great potential of this new material in catalysis.

**Keywords:** holey carbon material, hole defects, water-soluble, low bandgap, catalytic activity

## OPEN ACCESS

### Edited by:

Zhuhua Zhang,  
Nanjing University of Aeronautics and  
Astronautics, China

### Reviewed by:

Jincheng Lei,  
Yale University, United States  
Xiaodong Zhuang,  
Shanghai Jiao Tong University, China  
Ruiqi Zhao,  
Henan Polytechnic University, China

### \*Correspondence:

Yuzhou Liu  
liuyuzhou@buaa.edu.cn

<sup>†</sup>These authors have contributed  
equally to this work

### Specialty section:

This article was submitted to  
Physical Chemistry and Chemical  
Physics,  
a section of the journal  
Frontiers in Chemistry

**Received:** 20 January 2022

**Accepted:** 01 March 2022

**Published:** 21 March 2022

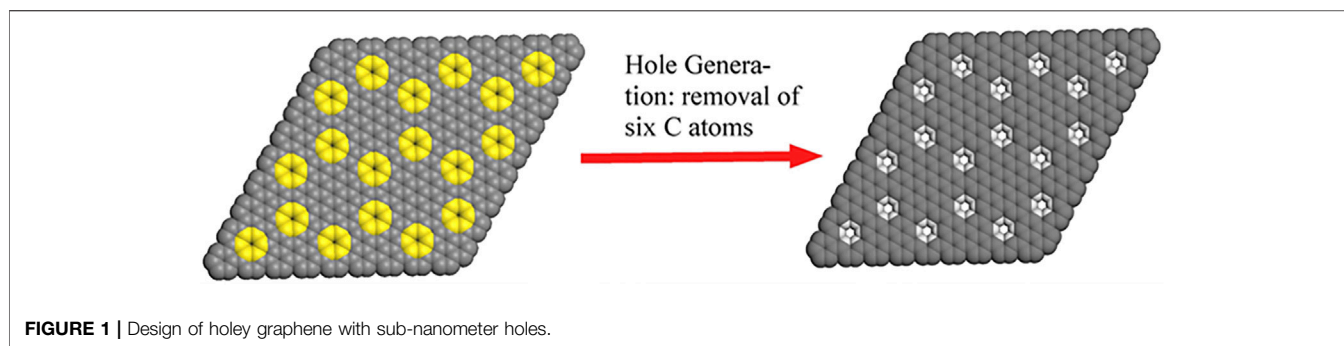
### Citation:

Liang N, Li Q, Pan G, Liu C and Liu Y  
(2022) Carbon Material With Ordered  
Sub-Nanometer Hole Defects.  
Front. Chem. 10:858154.  
doi: 10.3389/fchem.2022.858154

## INTRODUCTION

Graphene has garnered interest from people from all disciplines, because of its peculiar two-dimensional carbon-based conjugated structure (Geim and Novoselov, 2007). Graphene is a two-dimensional structure with sp<sup>2</sup>-honeycomb carbon lattice (Song et al., 2013). The formation of  $\pi$  bonds in the graphene honeycomb lattice creates a closed shell electron system. The superposition of multiple closed electronic shell systems produces an interaction dominated by repulsion, resulting in weak electronic coupling between the layers (Berashevich and Chakraborty, 2011). The weak interlayer interaction of graphene gives it a wide range of properties and applications (Lebedeva et al., 2011). The change of the force between graphene layers will have an important impact on its properties. Enhancing the interlayer interaction of bilayer graphene can effectively modulate the thermal transport (Sun et al., 2019). As the number of graphene layers increases, the interaction energy changes, and the room temperature thermal conductivity drops sharply (Ghosh et al., 2010). The interaction of bilayer graphene significantly changes the zero-field electronic structures, and has more abundant optical properties than monolayer graphene (Ho et al., 2010). Interlayer interaction will also affect the hydrogenation rate and selective etching (Imamura and Saiki, 2014). Exploring the interaction energy between graphene layers will help to prepare materials with novel functions.

The interlayer interaction of graphene is closely related to the dispersion of graphene. The energy barrier is introduced through electrostatic or steric repulsion to achieve electrostatically stability or steric stability and maintain a dispersion (Johnson et al., 2015; Hong et al., 2012). Many methods can be used to increase the dispersion of graphene. The graphite exfoliation (Yi et al., 2013; Bourlinos et al., 2009), microwave-assisted synthesis and functional modification methods can increase the dispersibility of graphene in water (Li et al., 2019; Long et al., 2011; Zuo et al., 2010; Wang et al., 2020; Jiang et al., 2019). By changing the solvent, graphite oxide can be stably dispersed in organic solvents (Mu et al., 2021), such as N,N-dimethylformamide (DMF) and tetrahydrofuran (THF). This can be explained as the polarity of the solvent molecules and graphene oxide sheets are comparable (Paredes



et al., 2008). The selective adsorption of functional groups on graphene can increase its dispersibility in suitable solvents. The 1,3-dipole cycloaddition can make graphene layers have higher dispersibility in water and DMF (Quintana et al., 2013). These methods affect the interlayer interaction of graphene, thereby improving the dispersion properties of graphene.

Graphene with sub-nanopores has a wide range of applications in ion transport (Suk and Aluru, 2014), selective ion sieving (van Deursen et al., 2019), seawater desalination (Xu et al., 2019), supercapacitors (Lee et al., 2016), etc., Graphene with nanopores has a strong water permeability and can be used as a reverse osmosis desalination membrane (Cohen-Tanugi and Grossman, 2014). The incorporation of three-dimensional nanopore crystals with sub-nano sized aperture size into the two-dimensional graphene laminate greatly improves the separation performance of water (Guan et al., 2017). Carbon materials with rich topological defects of high entropy have great potential in the field of electrocatalysis (Feng and Zhuang, 2020; Ding et al., 2021; Feng and Zhuang, 2021). Herein we would like to report our work of bulk synthesis of a graphene derivative with regular sub-nanometer defects. Correlation calculations confirm that its interlayer interaction energy is smaller than that of graphene, which leads to its unique dispersibility and electrocatalytic properties. Experiments and density functional theory (DFT) calculations confirmed that it can be dissolved in water well. Our work provides a new method for the dispersion and trapping of metal atoms in graphene in water.

## PREPARATION AND BANDGAP OF POLYHEXABENZOCORONENE NETWORK

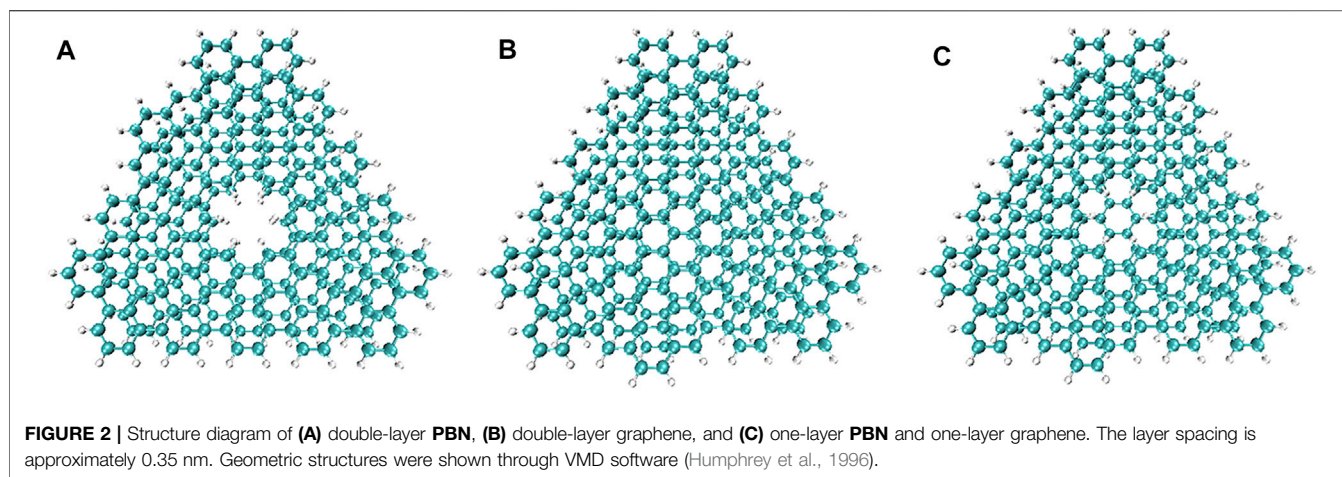
For bottom-up approach, the reaction condition in solution is much milder than that in previous top-down approaches, the formed small holes, which is found to self-heal under the high energy electron beam (Zan et al., 2012), are then expected to survive during the synthesis (Bieri et al., 2009). In addition, bottom-up approach offers structural precision and future tunability, since their structure follows deterministically from small-molecule precursors readily modified through organic synthesis. As shown in **Figure 1**, the removal of six adjacent carbons periodically from graphene layer will generate a holey graphene with sub-nanometer holes and hexabenzocoronene subunits. The hexabenzocoronene subunits are intentionally

targeted due to the fact that relative hexaphenylbenzene precursors can be readily made. The careful design leads to extremely simple experimental procedure, and we surprisingly found that the designed holey graphene structure can be easily made in bulk through simple oxidation reaction of a topologically equivalent polyhexaphenylbenzene network (PHN). Upon being soaked in the  $\text{CH}_2\text{Cl}_2$  solution of  $\text{FeCl}_3$  at room temperature, white PHN powder turned into dark brown immediately, which indicated the occurrence of the cyclodehydrogenation reaction. Finally, we obtained the anticipated polyhexabenzocoronene network (PBN). More synthetic details and structural confirmation are provided in our another manuscript (Liu et al., 2022).

PBN has a bandgap of around 2.2 eV, which matches very well with the calculated 2.1 eV at the HSE06 level and has a high accuracy in predicating bandgap energy. The bandgap is significantly reduced from those of hexabenzocoronene derivatives (2.7 ~ 3 eV) (Hiszpanski et al., 2015; Hughes et al., 2012; Davy et al., 2016), again reflecting the highly conjugated nature of PBN. From the point of view of holey graphene, the bandgap of this 2D hole-decorated graphene is justified by the narrow bridges between adjacent hexabenzocoronene units, whose width is inversely proportional to bandgap value (Son et al., 2006).

## INTERLAYER INTERACTION ENERGY OF POLYHEXABENZOCORONENE NETWORK

Non-covalent interactions, including  $\pi$ - $\pi$  interactions and van der Waals forces, are related to the dispersion of graphene (Georgakilas et al., 2016). Studying the non-covalent interaction between graphene and PBN can help explain the difference in the properties of the two. Independent gradient model (IGM) analysis, a method based on electron density (ED), can identify and isolate the interaction between user-defined fragments, using pro-molecular density (Lefebvre et al., 2017; Lu and Chen, 2022). Three models of double-layer PBN, double-layer graphene, one-layer PBN and one-layer graphene were considered to explore the difference of non-covalent interaction between PBN and graphene layers, as shown in **Figure 2**. The AA stacking structures were employed to qualitatively analyze the differences between the different models, ignoring the effect of different stacking models. The

**TABLE 1** | Interaction energy statistics of different models.

Energy	Double-layer PBN	Double-layer graphene	One-layer PBN and one-layer graphene
$E_{total}$ (au)	-11167.97	-11618.09	-11393.03
$E_{layer1}$ (au)	-5588.86	-5808.91	-5808.91
$E_{layer2}$ (au)	-5583.86	-5808.91	-5583.86
$E_{interaction}$ (eV/atom)	-0.0179	-0.0192	-0.0188

structure of the model was optimized first, and then the optimized structure was analyzed by IGM.

The structure optimization and single point energy calculation were performed with the ORCA package (Neese, 2012; Neese, 2018). The calculation used the BLYP functional, the def2-SVP basis set and the def2-SVP/J auxiliary basis set. The DFT-D3 dispersion correction with the Becke-Johnson damping function and tight SCF convergence criteria were used for calculation (Grimme et al., 2010; Grimme, 2011; Grimme et al., 2011; Becke and Johnson, 2006). The calculation solved the basis set superposition error (BSSE) problem by performing the geometrical Counterpoise Correction (gCP) at the level of a compound of the DFT and the def2-SVP basis set. The final single point energies after gCP correction of the three models and the individual layers of each model were counted. In order to describe the interaction energy between PBN or graphene, we define the interaction energy ( $E_{interaction}$ ) as:

$$E_{interaction} = (E_{total} - E_{layer1} - E_{layer2}) / N_{atoms}$$

where  $E_{total}$  represents the total energy of the three models,  $E_{layer1}$  and  $E_{layer2}$  represent the energy of PBN or graphene and  $N_{atoms}$  represents the total number of atoms of the three models.

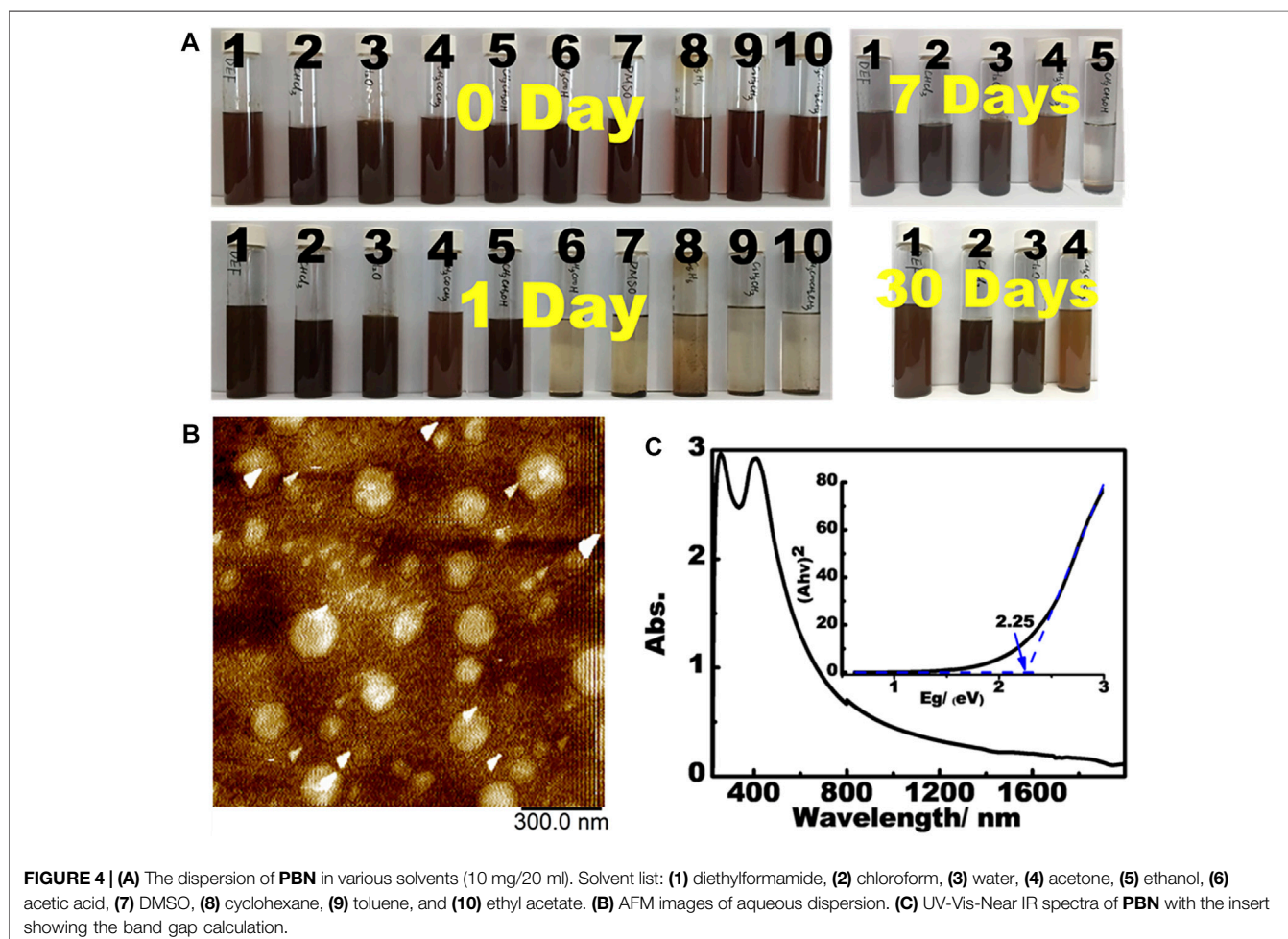
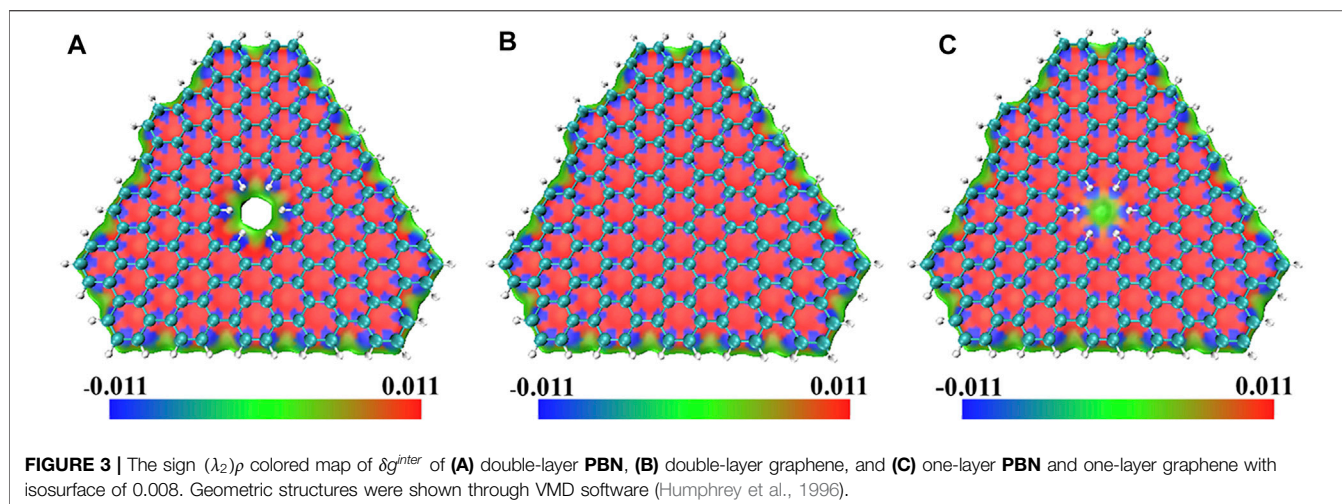
It can be seen from **Table 1** that the interlayer interaction energy of double-layer PBN is smaller than that of double-layer graphene, indicating that the existence of pores has an impact on non-covalent interaction. The interaction energy between one-layer PBN and one-layer graphene is slightly smaller than that of a double layer of graphene, indicating that the non-covalent interaction between the two pores is more obvious. In order to

further explore the influence of pores on non-covalent interactions, IGM analyses were performed on the three optimized models using Multiwfn software 3.7 (Lu and Chen, 2012). In IGM analyses,  $\delta g^{inter}$  is used to describe the interaction between molecules, which is defined as:

$$\delta g^{inter} = |\nabla \rho^{IGM,inter}| - |\nabla \rho|$$

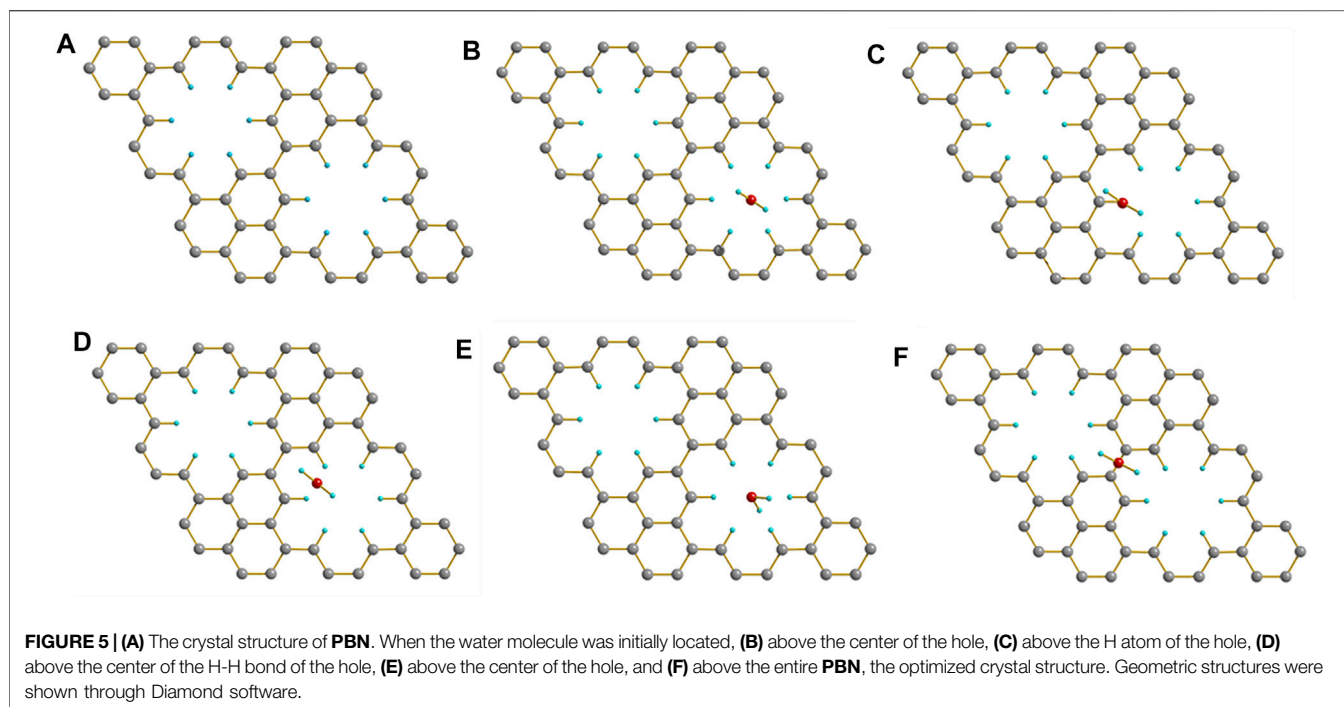
where  $|\nabla \rho|$  represents the norm of the ED gradient vector, and  $|\nabla \rho^{IGM,inter}|$  represents the upper limit of the independent gradient model when only the intermolecular interactions are cancelled. The sign of the Laplacian of the density,  $\nabla^2 \rho$ , can be decomposed into a sum of the contributions along the three principal axes of maximal variation. These components are the three eigenvalues  $\lambda_i$  ( $\lambda_1$ ,  $\lambda_2$  and  $\lambda_3$ ) of the ED Hessian (second derivative) matrix. The analysis of the sign of  $\lambda_2$  can help discern different types of noncovalent interactions, and  $\rho$  provides the strength of noncovalent interactions, so the product of the two was used for complete analyses of noncovalent interactions (Johnson et al., 2010). Regarding the two layers of the three models in **Figure 2** as two fragments for IGM analyses, the sign ( $\lambda_2$ ) $\rho$  colored isosurface map of  $\delta g^{inter}$  was shown in **Figure 3**.

In the blue area in **Figure 3**, the value of the sign ( $\lambda_2$ ) $\rho$  was small and there was a strong attraction effect, where the value of the sign ( $\lambda_2$ ) $\rho$  is close to 0, where there was van der Waals effect, and where the value of the sign ( $\lambda_2$ ) $\rho$  was large, there was a strong mutual repulsion effect (Lu and Chen, 2021). In the vertical structure of the upper and lower layers, there was a strong attraction between the atom pairs, and there was a strong mutual repulsion in the hexahedral structure surrounded by



carbon atoms. Where H atoms existed, such as holes and the edges of the system, there were Van der Waals forces. The existence of pores caused the non-covalent interaction to change from strong repulsion to van der Waals interaction,

which reduced the interlayer interaction energy. This effect was only obvious in the vicinity of the pores. The weak interlayer interaction energy leads to some unique properties of PBN.



## DISPERSION OF POLYHEXABENZOCORONENE NETWORK

**PBN** can be readily dispersed in a wide range of solvents. Unlike graphene and most 2D materials, **PBN** spontaneously disperses in common organic solvents to form dark red dispersion upon sonication (**Figure 4A**). The stability of the dispersion is also adjustable by the choices of solvents, with the dispersant ability roughly following the order of DEF,  $\text{CHCl}_3$ ,  $\text{H}_2\text{O}$  > Acetone > Ethanol > HOAc, DMSO, cyclohexane, toluene, EtOAc. AFM analysis on the aqueous dispersion show plates with the heights of 1~2 nm and diameters of up to 200 nms (**Figure 4B**), reflecting the few-layer dispersion in water. As far as we know, **PBN** represents the first 2D material that form stable dispersion in both hydrophobic and hydrophilic solvents without any additives. The simple and easy dispersion of **PBN** in a wide range of solvents up to single-layer level represents a significant advance in dispersible 2D materials (Marco et al., 2017). We suspect that the presence of sub-nanometer holes reduces inter-layer interaction while providing strong interaction with some specific small molecules. DFT calculations were performed to understand the dispersion of **PBN** in water.

All dispersion calculations of **PBN** were performed using the Vienna Ab initio Simulation Package (VASP) code (Kresse and Hafner, 1994; Kresse and Furthmüller, 1996). The Perdew–Burke–Ernzerhof (PBE) generalized gradient approximation (GGA) functional and the projected augmented wave (PAW) potential were used to describe the exchange–correlation potential and the ion–electron interactions, respectively. (Perdew et al., 1996; Kresse and Joubert, 1999). The kinetic energy cutoff for the plane-wave base was set to 500 eV and a  $2 \times 2 \times 1$  Gamma k-point mesh was

used to sample **PBN** and  $\text{H}_2\text{O}$  molecules. In the case of a fixed unit cell volume, the convergence criterion of  $10^{-4}$  eV for electron energy and convergence criterion of  $10^{-2}$  eV/Å for the forces on each ion were used to optimize all structures. The Many-body dispersion energy method (MBD@rsSCS) was used to determine the interaction energy of **PBN** and water molecules to account for van der Waals interactions (Lebègue et al., 2010).

In the optimization process of **PBN** and  $\text{H}_2\text{O}$  structure, we chose gaussian smearing to decide how to set the partial occupancies for each orbital. For the optimized structure, tetrahedron method with Blchl corrections was selected for accurate energy calculation, and the structures of **PBN** and  $\text{H}_2\text{O}$  were extracted from it, and the same method was used for energy calculation. In order to describe the interaction energy between **PBN** and water, we define the adsorption energy ( $E_{ads}$ ) as:

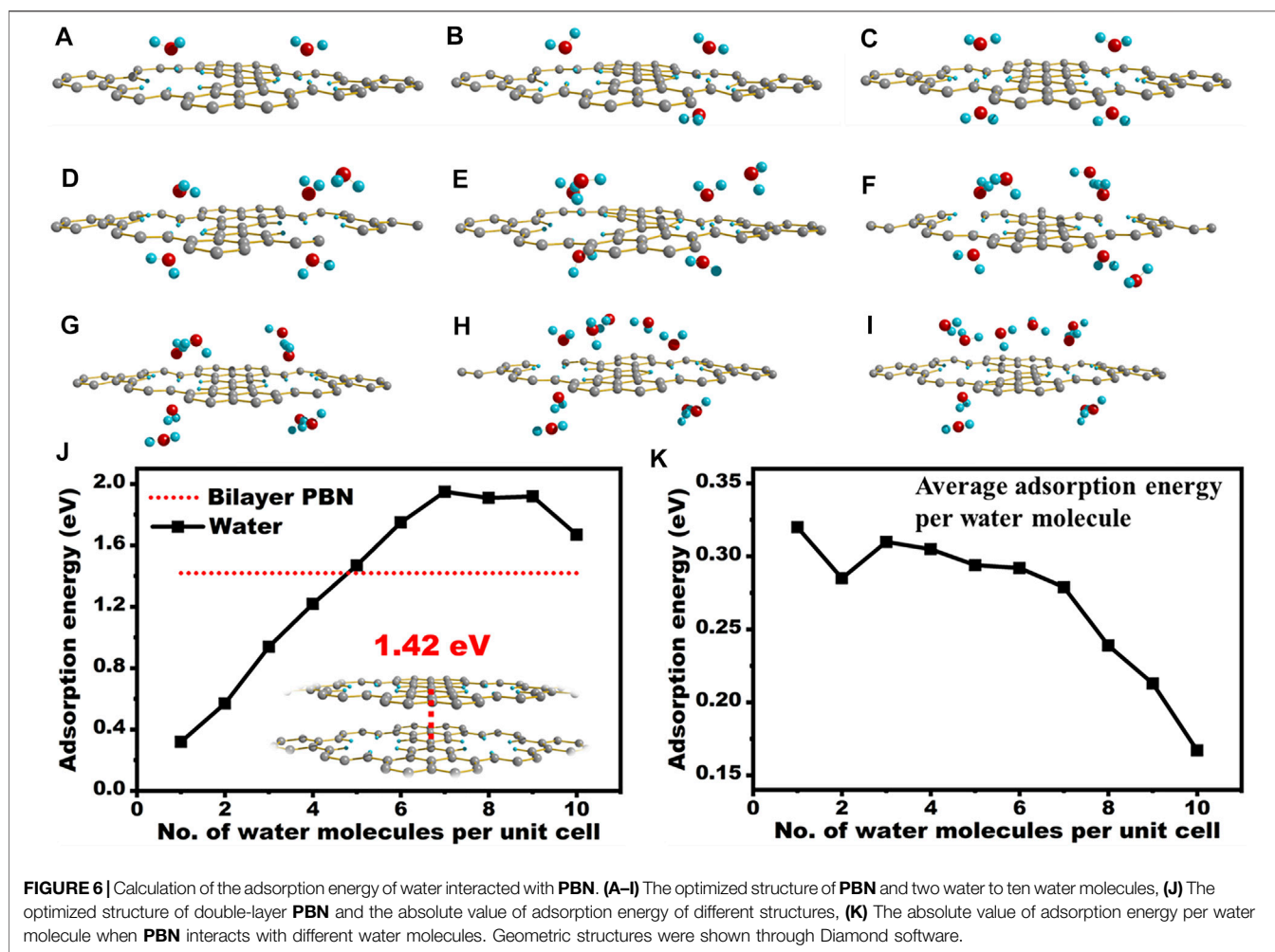
$$E_{ads} = E_{PBN+H_2O} - E_{PBN} - E_{H_2O}$$

where  $E_{PBN+H_2O}$  represents the total energy of **PBN** and water, and  $E_{PBN}$  and  $E_{H_2O}$  represent the energy of **PBN** and water respectively.

When **PBN** adsorbed a water molecule, the initial structure and the adsorption energy of the water molecule at different positions is shown in **Figure 5**. The **Figures 5B–E** are similar, indicating that the water molecules above the hole will automatically gather to the center of the hole during the optimization process. The holes may have a certain effect on the accumulation of water molecules. In comparison, the adsorption energy was only 0.06 eV when the adsorption site was nearby the center of hexabenzocoronene units, which was actually not unexpected given the bad solubility of large CH

**TABLE 2** | The adsorption energy of water at different positions.

Energy	Above the center of the hole	Above the H atom of the hole	Above the center of the H-H bond of the hole	Above the center of the hole	Above the entire PBN
$E_{PBN+H_2O}$ (eV)	-443.78	-443.78	-443.78	-443.79	-443.52
$E_{PBN}$ (eV)	-429.24	-429.24	-429.24	-429.24	-429.24
$E_{H_2O}$ (eV)	-14.22	-14.22	-14.22	-14.22	-14.22
$E_{ads}$ (eV)	-0.31	-0.32	-0.31	-0.32	-0.06



aromatics in water. Therefore, the presence of CH decorated holes is crucial to the strong interaction of PBN with water molecules.

The adsorption energy of PBN with different positions of water is shown in Table 2. The optimized results and the adsorption energy of the first four cases in Table 2 are similar, and they are all greater than the adsorption energy of the last case, indicating that when H<sub>2</sub>O is above the pores, PBN has a significant adsorption effect on water. In order to investigate the water solubility of PBN, the adsorption energy between PBN

and multiple water molecules and double-layer PBN was calculated, as shown in Figure 6.

DFT investigation of the interaction of PBN layer with water molecules revealed the interesting role of these sub-nanometer holes. The adsorption energy of one water molecule nearby the holes was around 0.32 eV or 7.34 kcal/mol, which was comparable to or even stronger than common hydrogen bond. In fact, the hydrogen bonding between two water molecules was estimated to be around 0.2 eV. This strong interaction will withdraw water molecule to the vicinity of PBN from the bulk

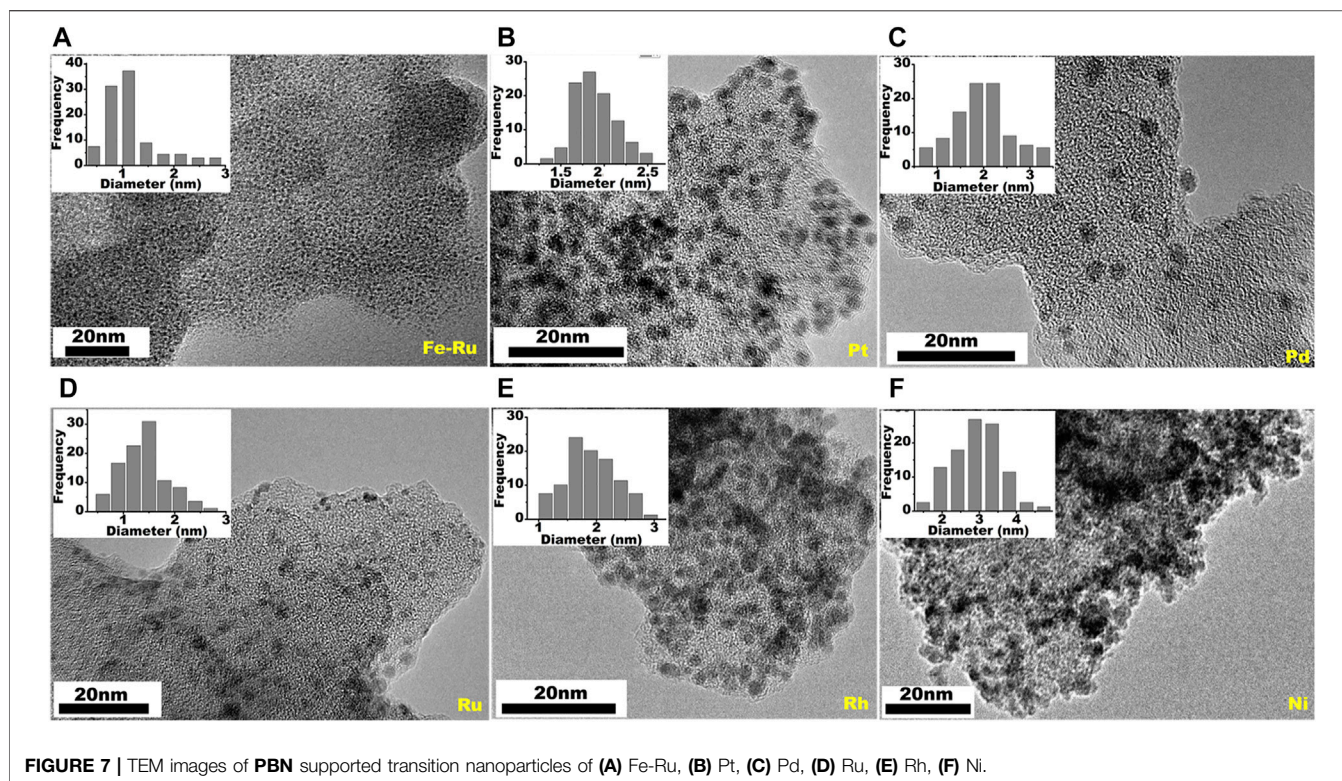


**FIGURE 7 |** TEM images of **PBN** supported transition nanoparticles of **(A)** Fe-Ru, **(B)** Pt, **(C)** Pd, **(D)** Ru, **(E)** Rh, **(F)** Ni.

solution. We further increased the number of water molecules per unit cell to probe maximum interaction per hole with water. With the increased in the number of water molecules around the **PBN** pores, the adsorption energy of **PBN** gradually increased, but the increasing trend gradually became flat. When it increased to about five waters, the adsorption energy of **PBN** and water molecules was greater than the interaction energy of double-layer **PBN** molecules. As shown in **Figure 6J**, as more water molecules were placed around the hole, the overall adsorption energy increased almost linearly to 1.9 eV. Excess water molecules may decrease the average adsorption energy per water molecule due to the formation of clusters (**Figure 6K**). We also computed the interlayer interaction of **PBN**, which was around 1.4 eV per unit cell, and it was actually smaller than the interaction between **PBN** and five water molecules. This explained the good dispersion of **PBN** in water.

## APPLICATION OF POLYHEXABENZOCORONENE NETWORK IN CATALYSIS

Treatment of unwashed **PBN**, which is loaded with  $\text{FeCl}_2$ , with excessive  $\text{NaBH}_4$  in ethanol leads **PBN** supported Fe NPs. The low atomic number of Fe prevents direct imaging, but galvanic replace of  $\text{Fe}^{2+}$  by  $\text{Ru}^{3+}$  leads to clear view of the extremely small nano Fe particles with sizes around 1 nm (**Figure 7A**) (Hudson et al., 2015), expected size value from the quantitative cyclodehydrogenation of polyhexaphenylbenzene network (**PHN**). We further take advantage of the feasible dispersion of

**PBN** to combine with various metal precursors in solution in order to expand the scope of loaded NPs. Interestingly, various **PBN**-NPs can be easily prepared simply by chemical reduction of relative metal salts in ethanol in the presence of **PBN**. This simple procedure leads to preparation of supported Pt, Pd, Ru, Rh, and Ni NPs by **PBN** (**Figure 7**). The sizes of the NPs range from 2 to 5 nm, reflecting the effective confinement of the growth of inorganic NPs by **PBN**. The wide range of supported NPs is consistent with previous DFT calculation which predicates strong interaction between small graphene defects and different various clusters (Navalon et al., 2016).

The use of these semiconducting **PBN** supported transition metal NPs was preliminarily tested on the reduction of nitrobenzene by  $\text{NaBH}_4$  by use of **PBN-FeCl<sub>2</sub>** at room temperature. **PBN-FeCl<sub>2</sub>** exhibits a remarkably different catalysis behavior compared to pure  $\text{FeCl}_2$ , which show sluggish first-order reaction kinetics (**Figure 8A**) (MacNair et al., 2014). **PBN-FeCl<sub>2</sub>** showed both greatly improved reaction yield and speed at the same 10 wt% loading. The formation of aniline product reaches quantitative within 20 min and the reaction speed remains constant up to around 95% yield, a phenomenon belonging to the zero-order reaction kinetics.

The super performance of **PBN-FeCl<sub>2</sub>** may be attributed to several factors associated with unique properties of **PBN** mentioned above. First, the zero-order kinetics indicates that there is a strong substrate binding prior to the occurrence of the catalysis on the surface of the Fe NPs, very similar to the enzyme-substrate binding in enzyme catalysis (Koerner et al., 1959). In fact, the **PBN** dispersion in nitrobenzene is stable up to months

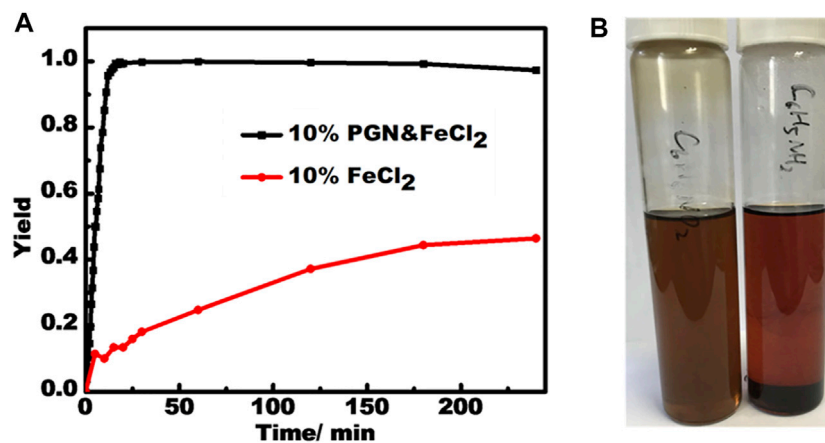


**FIGURE 8 | (A)** The reaction kinetics for catalysts of **PBN-FeCl<sub>2</sub>** and **FeCl<sub>2</sub>**. **(B)** The dispersion solutions of **PBN** in nitrobenzene and aniline respectively after 2 h.

without significant settlement while **PBN** almost completely settles down in phenylamine within a few hours (**Figure 8B**). This dispersion phenomenon indicates the strong binding of reactant and weak binding of the product, a prerequisite for efficient enzyme-like catalysis. Second, together with the small sizes of Fe NPs, their naked nature without any extra functional groups offers more reactive sites to interact with reactants, and therefore speeding up the reaction. Third, the semiconducting nature of **PBN** and its close contact with the Fe nanoparticles may change the electronic nature on the surface through the Mott-Schottky hetero junctions (Su et al., 2017). In addition, filtration test was conducted to validate the nature of heterogeneous catalysis by **PBN-FeCl<sub>2</sub>**.

In addition to its promise in next-generation graphene-based heterogeneous catalysts, **PBN** is also attractive for application in gas-filtration (Jiang et al., 2009), water-desalination (Cohen-Tanugi and Grossman, 2012), semiconductor devices (Kim et al., 2011), electromechanical sensors et al. (Boland Connor et al., 2016). where sub-nanometer holes, band-gap or feasible dispersion is required, indicating a wide application space.

## CONCLUSION

In conclusion, a holey carbon material with ordered sub-nanometer hole defects (polyhexabenzocoronene network, **PBN**) was synthesized by oxidative cyclodehydrogenation with polyhexaphenylbenzene as precursor. The IGM analyses of **PBN** and graphene show that **PBN** has weak interlayer interaction energy compared with graphene, which makes **PBN** has better dispersion performance than graphene. The DFT calculations show that the holes in **PBN** will attract water molecules nearby. With the number of water molecules increased, the interaction energy between **PBN** and water gradually increased, and when it reached saturation, the interaction energy of **PBN** and water was greater than that of double-layer graphene, which confirmed the excellent dispersion of **PBN** in water. It is proved experimentally that **PBN** can be dissolved in many other solvents in addition to

water. **PBN** can effectively support various inorganic nanoparticles of small sizes, and when **PBN** supports iron nanoparticles, it has high catalytic activity in the reduction of nitrophenyl by  $\text{NaBH}_4$ , indicating that it has great potential in catalysis.

## DATA AVAILABILITY STATEMENT

The original contributions presented in the study are included in the article/**Supplementary Material**, further inquiries can be directed to the corresponding author.

## AUTHOR CONTRIBUTIONS

All the authors conceived the theme and method of the research, and discussed the data. NL, QL, GP, and CL wrote the manuscript. QL, GP, and CL carried out the experiments. NL carried out the theoretical calculations. YL reviewed and edited the manuscript. All authors approved the submitted version of the manuscript.

## FUNDING

This work was supported by Beihang University Research Fund 74004601, Youth 1000 Talent Fund KZ37029501, and the 111 Project (B14009). This research was supported by the high performance computing (HPC) resources at Beihang University and the DeepChem platform from Shenyunzhihe Company.

## SUPPLEMENTARY MATERIAL

The Supplementary Material for this article can be found online at: <https://www.frontiersin.org/articles/10.3389/fchem.2022.858154/full#supplementary-material>



## REFERENCES

- Becke, A. D., and Johnson, E. R. (2006). Exchange-hole Dipole Moment and the Dispersion Interaction: High-Order Dispersion Coefficients. *J. Chem. Phys.* 124, 014104. doi:10.1063/1.2139668
- Berashovich, J., and Chakraborty, T. (2011). On the Nature of Interlayer Interactions in a System of Two Graphene Fragments. *J. Phys. Chem. C* 115, 24666–24673. doi:10.1021/jp2095032
- Bieri, M., Treier, M., Cai, J., Ait-Mansour, K., Ruffieux, P., Gröning, O., et al. (2009). Porous Graphenes: Two-Dimensional Polymer Synthesis with Atomic Precision. *Chem. Commun.*, 6919–6921. doi:10.1039/b915190g
- Boland, C. S., Khan, U., Ryan, G., Barwich, S., Charifou, R., Harvey, A., et al. (2016). Sensitive Electromechanical Sensors Using Viscoelastic Graphene-Polymer Nanocomposites. *Science* 354, 1257–1260. doi:10.1126/science.aag2879
- Bourlinos, A. B., Georgakilas, V., Zboril, R., Steriotis, T. A., Stubos, A. K., and Trapalis, C. (2009). Aqueous-phase Exfoliation of Graphite in the Presence of Polyvinylpyrrolidone for the Production of Water-Soluble Graphenes. *Solid State. Commun.* 149, 2172–2176. doi:10.1016/j.ssc.2009.09.018
- Cohen-Tanugi, D., and Grossman, J. C. (2012). Water Desalination across Nanoporous Graphene. *Nano Lett.* 12, 3602–3608. doi:10.1021/nl3012853
- Cohen-Tanugi, D., and Grossman, J. C. (2014). Mechanical Strength of Nanoporous Graphene as a Desalination Membrane. *Nano Lett.* 14, 6171–6178. doi:10.1021/nl502399y
- Davy, N. C., Man, G., Kerner, R. A., Fusella, M. A., Purdum, G. E., Sezen, M., et al. (2016). Contorted Hexabenzocoronenes with Extended Heterocyclic Moieties Improve Visible-Light Absorption and Performance in Organic Solar Cells. *Chem. Mater.* 28, 673–681. doi:10.1021/acs.chemmater.5b04503
- Ding, J., Wu, D., Zhu, J., Huang, S., Rodríguez-Hernández, F., Chen, Y., et al. (2021). High-entropy Carbons: From High-Entropy Aromatic Species to Single-Atom Catalysts for Electrocatalysis. *Chem. Eng. J.* 426, 131320. doi:10.1016/j.cej.2021.131320
- Feng, B., and Zhuang, X. (2020). Carbon-Enriched Meso-Entropy Materials: from Theory to Cases. *Acta Chim. Sinica* 78, 833–847. doi:10.6023/A20050167
- Feng, B., and Zhuang, X. (2021). The Philosophy of Carbon: Meso-Entropy Materials. *Faraday Discuss.* 227, 80–90. doi:10.1039/c9fd00115h
- Geim, A. K., and Novoselov, K. S. (2007). The Rise of Graphene. *Nat. Mater.* 6, 183–191. doi:10.1038/nmat1849
- Georgakilas, V., Tiwari, J. N., Kemp, K. C., Perman, J. A., Bourlinos, A. B., Kim, K. S., et al. (2016). Noncovalent Functionalization of Graphene and Graphene Oxide for Energy Materials, Biosensing, Catalytic, and Biomedical Applications. *Chem. Rev.* 116, 5464–5519. doi:10.1021/acs.chemrev.5b00620
- Ghosh, S., Bao, W., Nika, D. L., Subrina, S., Pokatilov, E. P., Lau, C. N., et al. (2010). Dimensional Crossover of thermal Transport in Few-Layer Graphene. *Nat. Mater.* 9, 555–558. doi:10.1038/nmat2753
- Grimme, S. (2011). Density Functional Theory with London Dispersion Corrections. *Wires Comput. Mol. Sci.* 1, 211–228. doi:10.1002/wcms.30
- Grimme, S., Antony, J., Ehrlich, S., and Krieg, H. (2010). A Consistent and Accurate Ab Initio Parametrization of Density Functional Dispersion Correction (DFT-D) for the 94 Elements H-Pu. *J. Chem. Phys.* 132, 154104. doi:10.1063/1.3382344
- Grimme, S., Ehrlich, S., and Goerigk, L. (2011). Effect of the Damping Function in Dispersion Corrected Density Functional Theory. *J. Comput. Chem.* 32, 1456–1465. doi:10.1002/jcc.21759
- Guan, K., Zhao, D., Zhang, M., Shen, J., Zhou, G., Liu, G., et al. (2017). 3D Nanoporous Crystals Enabled 2D Channels in Graphene Membrane with Enhanced Water Purification Performance. *J. Membr. Sci.* 542, 41–51. doi:10.1016/j.memsci.2017.07.055
- Hiszpanski, A. M., Saathoff, J. D., Shaw, L., Wang, H., Kraya, L., Lüttich, F., et al. (2015). Halogenation of a Nonplanar Molecular Semiconductor to Tune Energy Levels and Bandgaps for Electron Transport. *Chem. Mater.* 27, 1892–1900. doi:10.1021/acs.chemmater.5b00329
- Ho, Y. H., Wu, J. Y., Chiu, Y. H., Wang, J., and Lin, M. F. (2010). Electronic and Optical Properties of Monolayer and Bilayer Graphene. *Phil. Trans. R. Soc. A.* 368, 5445–5458. doi:10.1098/rsta.2010.0209
- Hong, B. J., Compton, O. C., An, Z., Eryazici, I., and Nguyen, S. T. (2012). Successful Stabilization of Graphene Oxide in Electrolyte Solutions: Enhancement of Biofunctionalization and Cellular Uptake. *ACS Nano* 6, 63–73. doi:10.1021/nn202355p
- Hudson, R., Chazelle, V., Bateman, M., Roy, R., Li, C.-J., and Moores, A. (2015). Sustainable Synthesis of Magnetic Ruthenium-Coated Iron Nanoparticles and Application in the Catalytic Transfer Hydrogenation of Ketones. *ACS Sust. Chem. Eng.* 3, 814–820. doi:10.1021/acssuschemeng.5b00206
- Hughes, J. M., Hernandez, Y., Aherne, D., Doessel, L., Müllen, K., Moreton, B., et al. (2012). High Quality Dispersions of Hexabenzocoronene in Organic Solvents. *J. Am. Chem. Soc.* 134, 12168–12179. doi:10.1021/ja303683v
- Humphrey, W., Dalke, A., and Schulten, K. (1996). VMD: Visual Molecular Dynamics. *J. Mol. Graphics* 14, 33–38. doi:10.1016/0263-7855(96)00018-5
- Imamura, G., and Saiki, K. (2014). Interlayer Interaction in the UV Irradiated Defect Formation of Graphene. *J. Phys. Chem. C* 118, 11842–11848. doi:10.1021/jp503802d
- Jiang, D.-e., Cooper, V. R., and Dai, S. (2009). Porous Graphene as the Ultimate Membrane for Gas Separation. *Nano Lett.* 9, 4019–4024. doi:10.1021/nl9021946
- Jiang, H.-B., Liu, Y., Liu, J., Li, S.-Y., Song, Y.-Y., Han, D.-D., et al. (2019). Moisture-Responsive Graphene Actuators Prepared by Two-Beam Laser Interference of Graphene Oxide Paper. *Front. Chem.* 7, 464. doi:10.3389/fchem.2019.00464
- Johnson, E. R., Keinan, S., Mori-Sánchez, P., Contreras-García, J., Cohen, A. J., and Yang, W. (2010). Revealing Noncovalent Interactions. *J. Am. Chem. Soc.* 132, 6498–6506. doi:10.1021/ja100936w
- Johnson, D. W., Dobson, B. P., and Coleman, K. S. (2015). A Manufacturing Perspective on Graphene Dispersions. *Curr. Opin. Colloid Interf. Sci.* 20, 367–382. doi:10.1016/j.cocis.2015.11.004
- Kim, K., Choi, J.-Y., Kim, T., Cho, S.-H., and Chung, H.-J. (2011). A Role for Graphene in Silicon-Based Semiconductor Devices. *Nature* 479, 338–344. doi:10.1038/nature10680
- Koerner, J. F., Smith, M. S., and Buchanan, J. M. (1959). A DEOXYCYTIDINE TRIPHOSPHATE SPLITTING ENZYME AND THE SYNTHESIS OF THE DEOXYRIBOSENUCLEIC ACID OF T2 BACTERIOPHAGE1. *J. Am. Chem. Soc.* 81, 2594–2595. doi:10.1021/ja01519a076
- Kresse, G., and Furthmüller, J. (1996). Efficient Iterative Schemes For ab Initio Total-Energy Calculations Using a Plane-Wave Basis Set. *Phys. Rev. B* 54, 11169–11186. doi:10.1103/PhysRevB.54.11169
- Kresse, G., and Hafner, J. (1994). Ab Initio Molecular-Dynamics Simulation of the Liquid-Metal-Amorphous-Semiconductor Transition in Germanium. *Phys. Rev. B* 49, 14251–14269. doi:10.1103/PhysRevB.49.14251
- Kresse, G., and Joubert, D. (1999). From Ultrasoft Pseudopotentials to the Projector Augmented-Wave Method. *Phys. Rev. B* 59, 1758–1775. doi:10.1103/PhysRevB.59.1758
- Lebedeva, I. V., Knizhnik, A. A., Popov, A. M., Lozovik, Y. E., and Potapkin, B. V. (2011). Interlayer Interaction and Relative Vibrations of Bilayer Graphene. *Phys. Chem. Chem. Phys.* 13, 5687–5695. doi:10.1039/c0cp02614j
- Lebègue, S., Harl, J., Gould, T., Ángyán, J. G., Kresse, G., and Dobson, J. F. (2010). Cohesive Properties and Asymptotics of the Dispersion Interaction in Graphite by the Random Phase Approximation. *Phys. Rev. Lett.* 105, 196401. doi:10.1103/PhysRevLett.105.196401
- Lee, K., Yoon, Y., Cho, Y., Lee, S. M., Shin, Y., Lee, H., et al. (2016). Tunable Subnanopores of Graphene Flake Interlayers with Conductive Molecular Linkers for Supercapacitors. *ACS Nano* 10, 6799–6807. doi:10.1021/acsnano.6b02415
- Lefebvre, C., Rubez, G., Khartabil, H., Boisson, J.-C., Contreras-García, J., and Hénon, E. (2017). Accurately Extracting the Signature of Intermolecular Interactions Present in the NCI Plot of the Reduced Density Gradient versus Electron Density. *Phys. Chem. Chem. Phys.* 19, 17928–17936. doi:10.1039/c7cp02110k
- Li, L., Zhou, M., Jin, L., Liu, L., Mo, Y., Li, X., et al. (2019). Research Progress of the Liquid-phase Exfoliation and Stable Dispersion Mechanism and Method of Graphene. *Front. Mater.* 6, 325. doi:10.3389/fmats.2019.00325
- Liu, C., Pan, G., Liang, N., Hong, S., Ma, J., and Liu, Y. (2022). Ir Single Atom Catalyst Loaded on Amorphous Carbon Materials with High HER Activity. *Adv. Sci.* 9. doi:10.1002/advs.202105392
- Long, J., Fang, M., and Chen, G. (2011). Microwave-assisted Rapid Synthesis of Water-Soluble Graphene. *J. Mater. Chem.* 21, 10421–10425. doi:10.1039/c0jm04564k
- Lu, T., and Chen, F. (2012). Multiwfn: A Multifunctional Wavefunction Analyzer. *J. Comput. Chem.* 33, 580–592. doi:10.1002/jcc.22885

- Lu, T., and Chen, Q. (2021). Interaction Region Indicator: A Simple Real Space Function Clearly Revealing Both Chemical Bonds and Weak Interactions\*\*. *Chem. Methods* 1, 231–239. doi:10.1002/cmt.202100007
- Lu, T., and Chen, Q. (2022). Independent Gradient Model Based on Hirshfeld Partition: A New Method for Visual Study of Interactions in Chemical Systems. *J. Comput. Chem.* 43, 539–555. doi:10.1002/jcc.26812
- MacNair, A. J., Tran, M.-M., Nelson, J. E., Sloan, G. U., Ironmonger, A., and Thomas, S. P. (2014). Iron-catalysed, General and Operationally Simple Formal Hydrogenation Using Fe(OTf)<sub>3</sub> and NaBH<sub>4</sub>. *Org. Biomol. Chem.* 12, 5082–5088. doi:10.1039/C4OB00945B
- Marco, A. B., Cortizo-Lacalle, D., Perez-Miqueo, I., Valenti, G., Boni, A., Plas, J., et al. (2017). Twisted Aromatic Frameworks: Readily Exfoliable and Solution-Processable Two-Dimensional Conjugated Microporous Polymers. *Angew. Chem. Int. Ed.* 56, 6946–6951. doi:10.1002/anie.201700271
- Mu, S., Yue, J., Wang, Y., and Feng, C. (2021). Electrical, Piezoresistive and Electromagnetic Properties of Graphene Reinforced Cement Composites: A Review. *Nanomaterials* 11, 3220. doi:10.3390/nano11123220
- Navalon, S., Dhakshinamoorthy, A., Alvaro, M., and Garcia, H. (2016). Metal Nanoparticles Supported on Two-Dimensional Graphenes as Heterogeneous Catalysts. *Coord. Chem. Rev.* 312, 99–148. doi:10.1016/j.ccr.2015.12.005
- Neese, F. (2012). The ORCA Program System. *Wires Comput. Mol. Sci.* 2, 73–78. doi:10.1002/wcms.81
- Neese, F. (2018). Software Update: the ORCA Program System, Version 4.0. *Wires Comput. Mol. Sci.* 8, e1327. doi:10.1002/wcms.1327
- Paredes, J. I., Villar-Rodil, S., Martínez-Alonso, A., and Tascón, J. M. D. (2008). Graphene Oxide Dispersions in Organic Solvents. *Langmuir* 24, 10560–10564. doi:10.1021/la801744a
- Perdew, J. P., Burke, K., and Ernzerhof, M. (1996). Generalized Gradient Approximation Made Simple. *Phys. Rev. Lett.* 77, 3865–3868. doi:10.1103/PhysRevLett.77.3865
- Quintana, M., Vazquez, E., and Prato, M. (2013). Organic Functionalization of Graphene in Dispersions. *Acc. Chem. Res.* 46, 138–148. doi:10.1021/ar300138e
- Son, Y.-W., Cohen, M. L., and Louie, S. G. (2006). Energy Gaps in Graphene Nanoribbons. *Phys. Rev. Lett.* 97, 216803. doi:10.1103/PhysRevLett.97.216803
- Song, X., Hu, J., and Zeng, H. (2013). Two-dimensional Semiconductors: Recent Progress and Future Perspectives. *J. Mater. Chem. C* 1, 2952–2969. doi:10.1039/c3tc00710c
- Su, H., Zhang, K.-X., Zhang, B., Wang, H.-H., Yu, Q.-Y., Li, X.-H., et al. (2017). Activating Cobalt Nanoparticles via the Mott-Schottky Effect in Nitrogen-Rich Carbon Shells for Base-free Aerobic Oxidation of Alcohols to Esters. *J. Am. Chem. Soc.* 139, 811–818. doi:10.1021/jacs.6b10710
- Suk, M. E., and Aluru, N. R. (2014). Ion Transport in Sub-5-nm Graphene Nanopores. *J. Chem. Phys.* 140, 084707. doi:10.1063/1.4866643
- Sun, Z., Yuan, K., Chang, Z., Zhang, X., Qin, G., and Tang, D. (2019). Efficient thermal Conductivity Modulation by Manipulating Interlayer Interactions: A Comparative Study of Bilayer Graphene and Graphite. *J. Appl. Phys.* 126, 125104. doi:10.1063/1.5115808
- van Deursen, P. M. G., Tang, Z., Winter, A., Mohn, M. J., Kaiser, U., Turchanin, A. A., et al. (2019). Selective Ion Sieving through Arrays of Sub-nanometer Nanopores in Chemically Tunable 2D Carbon Membranes. *Nanoscale* 11, 20785–20791. doi:10.1039/c9nr05537a
- Wang, B., Liu, Q., and Fan, Z. (2020). A Mini Review: Application Progress of Magnetic Graphene Three-Dimensional Materials for Water Purification. *Front. Chem.* 8, 595643. doi:10.3389/fchem.2020.595643
- Xu, G.-R., Xu, J.-M., Su, H.-C., Liu, X.-Y., Lu, L., Zhao, H.-L., et al. (2019). Two-dimensional (2D) Nanoporous Membranes with Sub-nanopores in Reverse Osmosis Desalination: Latest Developments and Future Directions. *Desalination* 451, 18–34. doi:10.1016/j.desal.2017.09.024
- Yi, M., Shen, Z., Liang, S., Liu, L., Zhang, X., and Ma, S. (2013). Water Can Stably Disperse Liquid-Exfoliated Graphene. *Chem. Commun.* 49, 11059–11061. doi:10.1039/c3cc46457a
- Zan, R., Ramasse, Q. M., Bangert, U., and Novoselov, K. S. (2012). Graphene Reknits its Holes. *Nano Lett.* 12, 3936–3940. doi:10.1021/nl300985q
- Zuo, X., He, S., Li, D., Peng, C., Huang, Q., Song, S., et al. (2010). Graphene Oxide-Facilitated Electron Transfer of Metalloproteins at Electrode Surfaces. *Langmuir* 26, 1936–1939. doi:10.1021/la902496u

**Conflict of Interest:** YL was employed by the company Beijing Shenyun Zhihe Technology Co., Ltd.

The remaining authors declare that the research was conducted in the absence of any commercial or financial relationships that could be construed as a potential conflict of interest.

**Publisher's Note:** All claims expressed in this article are solely those of the authors and do not necessarily represent those of their affiliated organizations, or those of the publisher, the editors and the reviewers. Any product that may be evaluated in this article, or claim that may be made by its manufacturer, is not guaranteed or endorsed by the publisher.

Copyright © 2022 Liang, Li, Pan, Liu and Liu. This is an open-access article distributed under the terms of the Creative Commons Attribution License (CC BY). The use, distribution or reproduction in other forums is permitted, provided the original author(s) and the copyright owner(s) are credited and that the original publication in this journal is cited, in accordance with accepted academic practice. No use, distribution or reproduction is permitted which does not comply with these terms.